Eur. Phys. J. B (2020) 93: 52
https://doi.org/10.1140/epjb/e2020-100492-6

THE EUROPEAN PHYSICAL JOURNAL B

Regular Article

A continuum model with traffic interruption probability and electronic throttle opening angle effect under connected vehicle environment

Cong Zhai[1,2] and Weitiao Wu[2,a]

[1] School of Transportation and Civil Engineering and Architecture, Foshan University, Foshan 528000, Guangdong, P.R. China
[2] School of Civil Engineering and Transportation, South China University of Technology, Guangzhou 510641, Guangdong, P.R. China

Received 9 October 2019 / Received in final form 15 January 2020
Published online 18 March 2020

Abstract. The electronic throttle system is the key component of the intelligent control system of connected and automated vehicles (CAVs). Although CAVs are expected to be commercialized in the near future, in practice the disturbances and interruptions are not uncommon along the road. In this paper, we propose a new continuum model considering the traffic interruption probability and the electronic throttle opening angle effect. Based on the linear stability analysis, the stability condition of the proposed model is obtained. The KdV-Burgers equation of the new continuum model is further obtained in the nonlinear analysis. The density solution obtained by solving the above equation can be used to describe the evolution characteristics of traffic flow near the neutral stability curve. Results show that the traffic interruption probability and the electronic throttle opening angle effect has a considerable impact on the stability of traffic flow.

1 Introduction

With the rapid development of the economy, there is increasing need for managing traffic congestion to ensure the operational efficiency and reduce traffic safety. On one hand, researchers have proposed a variety of traffic management strategies such as bus scheduling optimization to attract travelers from private cars to public transport [1–4]. On the other hand, there exist extensive studies on traffic flow and understand the mechanism and propagation of traffic congestion and propose proper traffic control strategies. This paper investigates the traffic flow models, more specifically the impact of a not uncommon but so far neglected traffic phenomenon on the traffic continuum model.

Generally, traffic flow models could be divided into two categories, namely the macro and micro traffic flow models. The subject of the former focuses on the regional traffic volume, which includes continuum models [5–10], and the hydrodynamic models [11–19]. The subject of the latter, however, focuses on the individual vehicle. The models includes the cellular automaton models [20,21], the car-following models [22–24], etc. Beginning with the seminal work of Bando [25] in 1995, an extensive literature has developed on the extended versions under different objectives and context, such as memory time [26–28]; anticipation time [29–32]; delay time [33–35]; driver characteristics [36–38]; multiple vehicle information [39–42]; optimal speed influence [43–45]; and traffic jerk [46–48].

With the advance of internet and communication technologies, the connected and automated vehicles (CAVs) are expected to become the mainstream of future transportation [49–54]. Notwithstanding that, the mass adoption of CAVs largely relies on the effective information communication, whereas the information communication between vehicles will be affected by many factors, such as the locations of base stations, traffic accidents, non-closed road pedestrian crossings, and other surrounding environment. On the other hand, in a connected vehicle environment, extensive information from the vehicles ahead is required to share within the vehicle platoon in order to avoid collisions. The opening angle of the electronic throttle (ET) of the vehicles ahead provides the opportunities for the following vehicles in the platoon to react autonomously to avoid collisions by adjusting its ET [55,56], which may in turn affect the vehicle speed. With an expectation that a variety of factors would exert influence on the transmission of real-time data and that ET adjustment relies on information communication, the traffic interruption and electronic throttle opening angle effect should be considered jointly in a traffic flow model under connected vehicle environment, which has significant implications in the realm of future transportation. However, this issue has not been fully addressed by the

[a] e-mail: ctwtwu@scut.edu.cn

existing macroscopic traffic flow models. This paper sets out to fill this gap.

The rest of this paper is organized as follows. In Section 2, an extended continuum model considering the traffic interruption probability and electronic throttle opening angle effect is proposed. In Section 3, the stability analysis is studied for the proposed model. Section 4 is devoted to nonlinear analysis and the derivation of the KdV-Burgers equation. In Section 5, we present the numerical example to verify the conclusion given in the theoretical analysis. Finally, we conclude the paper.

2 Model

In 1998, Bando proposed an optimal speed following model to describe the car-following behavior between vehicles on a single lane [25]. The model assumes that the vehicle's acceleration adjustment at the next moment is determined by the difference between the optimal speed and current speed of the vehicle, and the optimal speed of the vehicle is only determined by the current headway. The dynamic equation of the car-following model is presented as follows:

$$\frac{dv_n(t)}{dt} = a\left[V\left(\Delta x_n(t)\right) - v_n(t)\right] \tag{1}$$

where $v_n(t), \Delta x_n(t)$ is the instantaneous speed and headway of the nth car at time t, and $\Delta x_n(t) = x_{n+1}(t) - x_n(t)$; a is the driver's sensitivity; the term $V\left(\Delta x_n(t)\right)$ is the optimal speed function, which is only determined by the headway of the nth car at time t and expressed as follows:

$$V\left(\Delta x_n(t)\right) = \frac{v_{\max}}{2}\left[\tanh\left(\Delta x_n(t) - h_c\right) + \tanh\left(h_c\right)\right] \tag{2}$$

where $v_{\max}$ and h_c are the maximum speed and safety distance of the vehicles on the road, respectively.

Based on the field data, Helbing and Tilch [57] reported that the acceleration of vehicles in the OV model was generally too large, such that unreasonable deceleration and even collision exist. To overcome this drawback, they propose a general force model (GF)

$$\frac{dv_n(t)}{dt} = a\left[V\left(\Delta x_n(t)\right) - v_n(t)\right] + \gamma H(-\Delta v_n(t))\Delta v_n(t) \tag{3}$$

where γ is sensitivity coefficient; $H(\bullet)$ is the Heaviside function, which can be viewed as a typical type of continuous time function. This function reflects the transition process from 0 to 1, specifically $H(\bullet) = \begin{cases} 0, x \le 0 \\ 1, x > 0 \end{cases}$; $\Delta v_n(t)$ is the velocity difference of the n car at time t, and $\Delta v_n(t) = v_{n+1}(t) - v_n(t)$.

Later, Jiang [58] found that the starting velocity of the traffic flow was too small in the GF model. For this reason, they proposed the Full Velocity Difference Model (FVD)

$$\frac{dv_n(t)}{dt} = a\left[V\left(\Delta x_n(t)\right) - v_n(t)\right] + \lambda \Delta v_n(t). \tag{4}$$

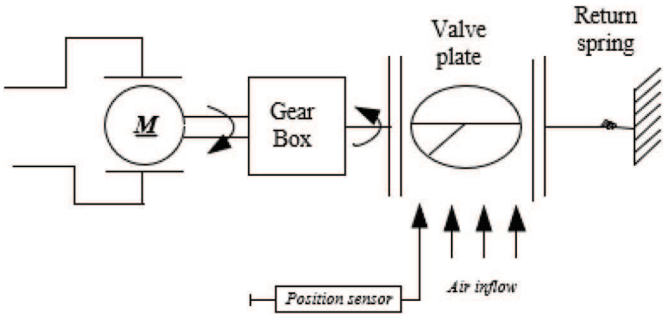

Fig. 1. The functional scheme of the ET.

Due to the simple structure and strong explanatory power of FVD, the model has gained wide popularity. However, the model cannot directly analyze the impact of traffic interruption on traffic stability. As discussed, the traffic interruption is ubiquitous including traffic accidents, pedestrian crossings, toll stations, signalized intersections, etc. To this end, Tang [59] presented an improved car-following model on the basis of equation (4), that is

$$\begin{aligned}\frac{dv_n(t)}{dt} = {} & a\left[V\left(\Delta x_n(t)\right) - v_n(t)\right] + k_1 p_n\left(-v_n(t)\right) \\ & + k_2\left(1 - p_n\right)\Delta v_n(t)\end{aligned} \tag{5}$$

where p_n represents the possibility of traffic interference in front of the nth vehicle. Since the possibility of traffic interruption would vary with the surrounding traffic environment, we assume a constant parameter in order to facilitate subsequent analysis, i.e., $p_n = p$. k_1 and k_2 represent the corresponding weight coefficient.

As the key components of the future CAV intelligent control system, the electronic throttle system consists of a DC drive (powered by the chopper), a gearbox, a valve plate, a dual return spring, and a position sensor. Figure 1 shows the functional scheme of the ET. The electronic throttle angle is closely related to the speed and acceleration of the vehicle. The feedback of the electronic throttle angle plays an important role in the real-time perception of the preceding vehicle running state, which improves the micro-following characteristics of the following vehicle. Recently, the effect of the electronic throttle opening angle was found to have a significant impact on traffic flow stability [55,56]. In light of this, the effect of ET opening angle is further incorporated into equation (5), then we have that:

$$\begin{aligned}\frac{dv_n(t)}{dt} = {} & a\left[V\left(\Delta x_n(t)\right) - v_n(t)\right] + k_1 p_n\left(-v_n(t)\right) \\ & + k_2\left(1 - p_n\right)\Delta v_n(t) + \beta \Delta \theta_n(t)\end{aligned} \tag{6}$$

where β is the weight coefficient of $\Delta\theta_n(t)$; $\Delta\theta_n(t)$ is the ET opening angle difference between $n+1$ vehicle and the n vehicle at time t, and $\Delta\theta_i(t) = \theta_{i+1}(t) - \theta_i(t)$.

Similar to the literature [55], the relationship between ET open angle information and acceleration and speed of

nth vehicle are measured as follows:

$$\frac{dv_n(t)}{dt} = -b\left[v_n(t) - v_0\right] + m\bar{\theta}_n + h_n \tag{7}$$

where $\bar{\theta}_n$ is the angle difference, and $\bar{\theta}_n = \theta_n - \theta_0$; θ_0 and v_0 represent the initial electronic throttle opening angle and initial velocity of vehicle, respectively; b and m is the weight coefficient of velocity difference and angle difference, respectively; h_n is the disturbance of non-modeled dynamics influence.

According to equation (7), the expression of ET opening angle difference can be obtained as follows:

$$\begin{aligned}\Delta\theta_n(t) &= \theta_{n+1}(t) - \theta_n(t) \\ &= \frac{1}{m}\left[\frac{dv_{n+1}(t)}{dt} - \frac{dv_n(t)}{dt} + b\Delta v_n(t)\right].\end{aligned} \tag{8}$$

In order to convert the microscopic variables into macro variables, we adopt the following transformation

$$v_n(t) \to v(x,t) v_{n+1}(t) \to v(x+\Delta, t) V\left(\Delta x_n(t)\right) \to V_e(\rho) \tag{9}$$

where Δ represents the distance between the two adjacent vehicles; $\rho(x,t)$ and $v(x,t)$ represent macroscopic density and macroscopic speed, respectively.

Subsequently, we perform a Taylor expansion on the variable $v(x+\Delta, t)$ while ignoring the higher-order nonlinear terms, then we have that:

$$\Delta v_n(t) = v(x+\Delta, t) - v(x,t) = v'(x,t)\Delta + \frac{1}{2}v''(x,t)\Delta^2 \tag{10}$$

$$\frac{du_{n+1}(t)}{dt} = uu_x + \Delta u_x u_x + u_t + \Delta u_{xt}. \tag{11}$$

Substituting equations (10) and (11) into equation (6), the following equation can be obtained:

$$\begin{aligned}&\frac{\partial v}{\partial t} + v\frac{\partial v}{\partial x} = a\left[V_e(\rho) - v\right] + k_1 p\left(-v\right) \\ &+\frac{k_2\left(1-p\right)m + b\beta}{m}\Delta v_n(t) + \frac{\beta}{m}\left[\Delta v_x v_x + \Delta v_{xt}\right].\end{aligned} \tag{12}$$

Converting the above formula, then we have

$$\begin{aligned}&\frac{\partial v}{\partial t} + \left[v - \frac{k_2(1-p)m + b\beta}{m}\Delta - \frac{\beta}{m}\Delta\frac{\partial v}{\partial x}\right]\frac{\partial v}{\partial x} = a\left[V_e(\rho) - v\right] \\ &+k_1 p\left(-v\right) + \frac{k_2(1-p)m + b\beta}{2m}v''(x,t)\Delta^2 + \frac{\beta}{m}\Delta v_{xt}.\end{aligned} \tag{13}$$

Combining equation (13) with conservative equation, then a new continuum model considering the traffic interruption probability and electronic throttle opening angle effect is presented:

$$\begin{cases}\frac{\partial \rho}{\partial t} + \rho\frac{\partial v}{\partial x} + v\frac{\partial \rho}{\partial x} = 0 \\ \frac{\partial v}{\partial t} + \left[v - c_0\right]\frac{\partial v}{\partial x} = a\left[V_e(\rho) - v\right] + k_1 p\left(-v\right) \\ \qquad\qquad + \frac{k_2(1-p)m + b\beta}{2m}v''(x,t)\Delta^2 + \frac{\beta}{m}\Delta v_{xt}\end{cases} \tag{14}$$

where $c_0 = \frac{k_2(1-p)m + b\beta}{m}\Delta + \frac{\beta}{m}\Delta\frac{\partial v}{\partial x}$.

3 Linear stability analysis

The purpose of this section is to analyze the model properties by using linear stability method. In order to facilitate subsequent analysis, equation (14) is first converted into the following vector format.

$$\frac{\partial U}{\partial t} + A\frac{\partial E}{\partial x} = E \tag{15}$$

where

$$U = \begin{bmatrix}\rho \\ v\end{bmatrix}, \quad A = \begin{bmatrix}v & \rho \\ 0 & v - c_0\end{bmatrix},$$

$$E = \begin{bmatrix}0 \\ a\left[V_e(\rho) - v\right] - k_1 pv + \frac{k_2(1-p)m + b\beta}{2m}v''(x,t)\Delta^2 + \frac{\beta}{m}\Delta v_{xt}\end{bmatrix}.$$

Solving the characteristic polynomial $|\lambda I - A| = 0$, the characteristic velocity can be obtained, namely,

$$\lambda_1 = v, \lambda_2 = v - c_0. \tag{16}$$

Since $k_2, \Delta, m, b, \beta > 0$ and $p_n \le 1$, $\lambda_1, \lambda_2 \le v$ can be obtained. This indicates that the characteristic speed is always smaller than the macroscopic traffic flow speed, such that the new continuum model is anisotropic.

In order to obtain the stability condition of the new continuum model, a small disturbance is put into the steady state of the model, i.e.,

$$\begin{pmatrix}\rho(x,t) \\ v(x,t)\end{pmatrix} = \begin{pmatrix}\rho_0 \\ v_0\end{pmatrix} + \sum\begin{pmatrix}\hat{\rho}_k \\ \hat{v}_k\end{pmatrix}\exp(ikx + \sigma_k t). \tag{17}$$

Substituting equation (17) into equation (14) and ignoring the higher-order nonlinear terms, then we have

See equation (18) next page.

As long as the coefficient determinant of equation (18) is equal to 0, there is a non-zero solution for $(\hat{\rho}_k, \hat{v}_k)$ in equation (18), that is

$$\begin{vmatrix}\sigma_k + v_0 ik & \rho_0 ik \\ & -\sigma_k - v_0 ik + \frac{k_2(1-p)m + b\beta}{m}\Delta ik \\ & -a - k_1 p + \frac{\beta}{m}\Delta\sigma_k ik \\ aV_e'(\rho_0) & +\frac{k_2(1-p)m + b\beta}{2m}\Delta^2\left(ik\right)^2\end{vmatrix} = 0. \tag{19}$$

$$\begin{cases} (\sigma_k + v_0 ik)\,\hat{\rho}_k + \rho_0 ik\hat{v}_k = 0 \\ aV_e'(\rho_0)\hat{\rho}_k + \left(-\sigma_k - v_0 ik + \frac{k_2(1-p)m+b\beta}{m}\Delta ik - a - k_1 p + \frac{\beta}{m}\Delta\sigma_k ik + \frac{k_2(1-p)m+b\beta}{2m}\Delta^2 (ik)^2 \right)\hat{v}_k = 0 \end{cases} \tag{18}$$

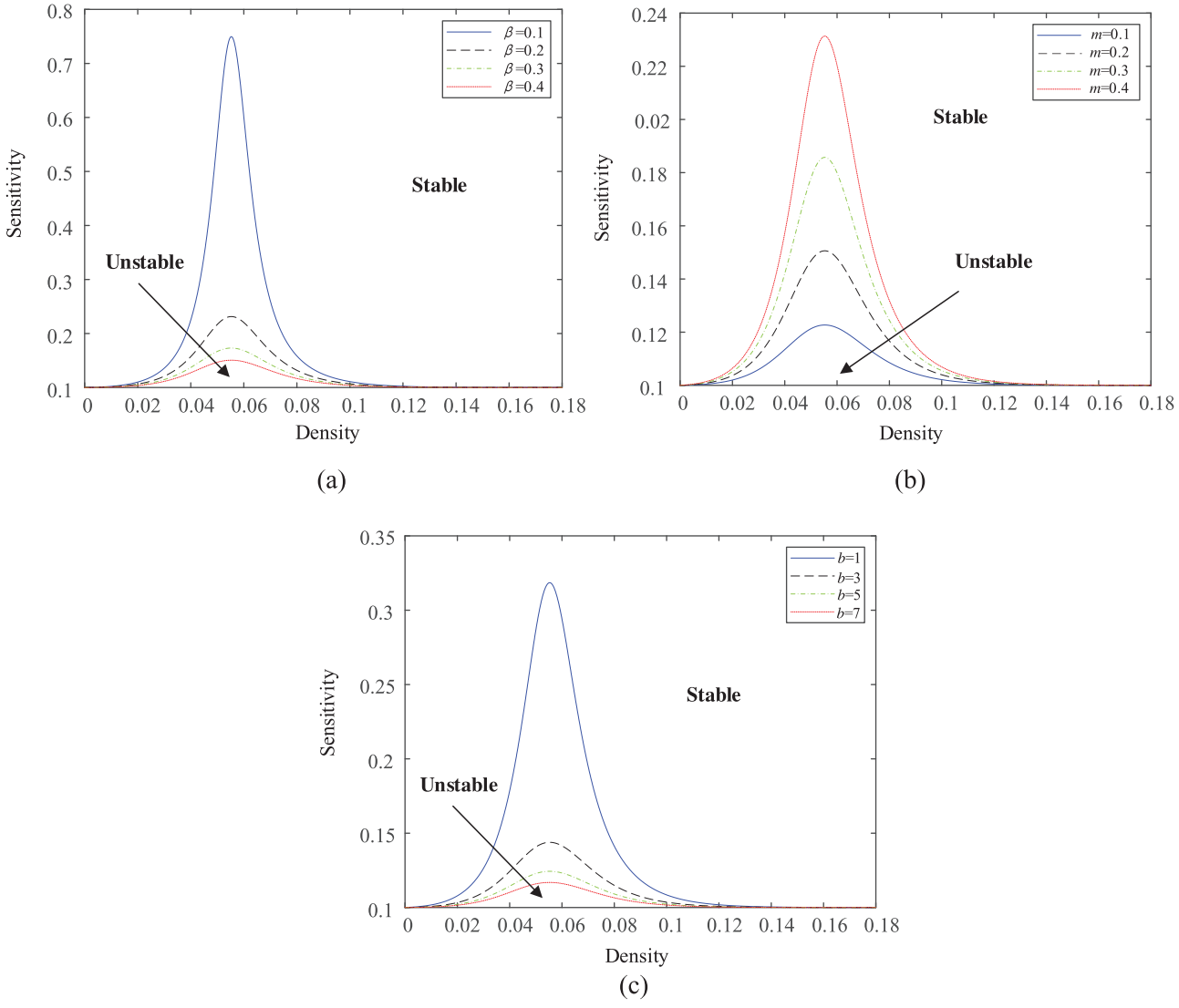

Fig. 2. The neutral stability curves under different parameters (a) β; (b) m; (c) b.

Solving the above determinant, it can be seen that σ_k satisfies the following quadratic equation, i.e.

$$\begin{aligned} &(\sigma_k + v_0 ik)^2 + (\sigma_k + v_0 ik) \\ &\times \left(\begin{array}{l} -\frac{k_2(1-p)m+b\beta}{m}\Delta ik + a + k_1 p - \\ \frac{\beta}{m}\Delta\sigma_k ik - \frac{k_2(1-p)m+b\beta}{2m}\Delta^2 (ik)^2 \end{array} \right) + aV_e'(\rho_0)\rho_0 ik \\ &= 0. \end{aligned} \tag{20}$$

The traffic flow is stable as long as σ_k has a negative real part. In order to determine the value of σ_k, we first perform a Taylor expansion of σ_k, specifically $\sigma_k = \sigma_1 ik + \sigma_2 (ik)^2 + \cdots$. In order to ensure that the equation holds, the coefficients of the first and second power series should be zero, such that σ_1 and σ_2 can be obtained, that is,

$$\begin{cases} \sigma_1 = -v_0 - (a + k_1 p)^{-1} a\rho_0 V_e'(\rho_0) \\ \sigma_2 = (a + k_1 p)^{-2} (a\rho_0 V_e'(\rho_0)) \left(\frac{k_2(1-p)m+b\beta}{m}\Delta \right) \\ \qquad - (a + k_1 p)^{-3} (a\rho_0 V_e'(\rho_0))^2 . \end{cases} \tag{21}$$

In order to make the system stable, $\sigma_2 > 0$ is required. As a result, the neutral stability curve of the system can be obtained

$$a = \frac{k_1 p \Delta \left[k_2 (1-p) m + b\beta\right]}{m\rho_0 u_e'(\rho_0) - \left[k_2 (1-p) m + b\beta\right] \Delta} \tag{22}$$

$$\mathrm{Im}(\sigma_k) = -k \left[v_0 + (a + k_1 p)^{-1} a\rho_0 V_e'(\rho_0)\right] + O(k^3). \tag{23}$$

Based on equation (23), the propagation speed c of the disturbance is

$$c_0(\rho_0) = v_0 + (a + k_1 p)^{-1} a\rho_0 V_e'(\rho_0). \tag{24}$$

When $p = 0$, then the conclusion is consistent with the conclusions presented in the literature [60–64].

Figure 2 shows the neutral stability curve of the new model under different parameters β, m, b. The stability area is above the neutral stability curve, which indicates that the traffic jams will not occur. On the contrary, the instability area is below the neutral stability curve, where traffic jam is likely to occur. As we can see, the stability area expands as the parameter β and b increase, which indicates the enhanced model stability. However, the effect of parameter m exhibits an opposite trend. Therefore, it can be concluded that the parameters β and b contributes to the stability of the model, whereas the parameter m contributes negatively.

4 Nonlinear stability analysis

The purpose of this section is to conduct a nonlinear stability analysis to understand the propagation process of small disturbances in the unstable area. As the initial density gradually increases, a small disturbance may evolve into various states, such as a single local cluster and multiple local clusters. The local clusters indicate the stop-and-go phenomenon. Based on the non-linear analysis, the fluctuating amplitude and propagation velocity of the stop-and-go wave can be obtained. To this end, we first introduce a new coordinate system as follows:

$$z = x - ct. \tag{25}$$

Putting equation (25) into equation (14), then we obtain

$$\begin{cases} -c\rho_z + q_z = 0 \\ -c\frac{\partial v}{\partial z} + \left[v - \frac{k_2(1-p)m+b\beta}{m}\Delta - \frac{\beta}{m}\Delta\frac{\partial v}{\partial z}\right]\frac{\partial v}{\partial z} \\ \quad = a\left[V_e(\rho) - v\right] + k_1 p\,(-v) \\ \quad\quad + \frac{k_2(1-p)m+b\beta}{2m}\Delta^2 v_{zz} - \frac{c\beta}{m}\Delta v_{zz} \end{cases} \tag{26}$$

where q represents the traffic flow, and $q = \rho \times v$.

Based on the first equation of equation (26), the following formulation is available

$$v_z = \frac{c\rho_z}{\rho} - \frac{q\rho_z}{\rho^2}. \tag{27}$$

Deriving v_z, then we obtain

$$v_{zz} = \frac{c\rho_{zz}}{\rho} - \frac{2c\rho_z^2}{\rho^2} - \frac{q\rho_{zz}}{\rho^2} + \frac{2q\rho_z^2}{\rho^3}. \tag{28}$$

In equation (28), the traffic flow q can be expressed as

$$q = \rho V_e(\rho) + b_1\rho_z + b_2\rho_{zz}. \tag{29}$$

Bringing equations (27)–(29) into equation (26), then

$$\begin{aligned} &-c\left(\frac{c\rho_z}{\rho} - \frac{q\rho_z}{\rho^2}\right) + \left[\frac{q}{\rho} - \frac{k_2(1-p)m+b\beta}{m}\Delta \right. \\ &\left. -\frac{\beta}{m}\Delta\left(\frac{c\rho_z}{\rho} - \frac{q\rho_z}{\rho^2}\right)\right]\left(\frac{c\rho_z}{\rho} - \frac{q\rho_z}{\rho^2}\right) \\ &= a\left[V_e(\rho) - \frac{q}{\rho}\right] + k_1 p_n\left(-\frac{q}{\rho}\right) \\ &\quad + \left(\frac{k_2(1-p)m+b\beta}{2m}\Delta^2 - \frac{c\beta}{m}\Delta\right) \\ &\quad \times \left(\frac{c\rho_{zz}}{\rho} - \frac{2c\rho_z^2}{\rho^2} - \frac{q\rho_{zz}}{\rho^2} + \frac{2q\rho_z^2}{\rho^3}\right). \end{aligned} \tag{30}$$

Since both ρ_z and ρ_{zz} are not zero, the coefficients of ρ_z and ρ_{zz} in equation (30) equal to 0, from which the following equations are obtained.

$$\begin{cases} b_1 = \frac{(c - V_e(\rho))\left[V_e(\rho) - \frac{k_2(1-p)m+b\beta}{m}\Delta - c\right]}{a + k_1 p} \\ b_2 = \frac{\left(\frac{k_2(1-p)m+b\beta}{2m}\Delta^2 - \frac{c\beta}{m}\Delta\right)(c - V_e(\rho))}{a + k_1 p}. \end{cases} \tag{31}$$

Near the neutral stability curve, let $\rho = \rho_h + \hat{\rho}(x,t)$, and perform a Taylor expansion on ρ to expand to the second-order term about $\hat{\rho}$, then we obtain

$$\rho u_e(\rho) \approx \rho_h u_e(\rho_h) + (\rho u_e)_\rho\Big|_{\rho=\rho_h}\hat{\rho} + \frac{1}{2}(\rho u_e)_{\rho\rho}\Big|_{\rho=\rho_h}\hat{\rho}^2. \tag{32}$$

Putting equation (32) into equation (30) and replacing $\hat{\rho}$ by ρ, then we have

$$-c\rho_z + \left[(\rho u_e)_\rho + (\rho u_e)_{\rho\rho}\rho\right]\rho_z + b_1\rho_{zz} + b_2\rho_{zzz} = 0. \tag{33}$$

In order to obtain the standard KdV-Burgers equation, equation (33) is transformed as follows

$$U = -\left[(\rho u_e)_\rho + (\rho u_e)_{\rho\rho}\rho\right], \quad X = mx, \quad T = -mt. \tag{34}$$

Substituting equation (34) into equation (33), the standard KdV-Burgers equation can be obtained

$$U_T + UU_X - mb_1 U_{XX} - m^2 b_2 U_{XXX} = 0. \tag{35}$$

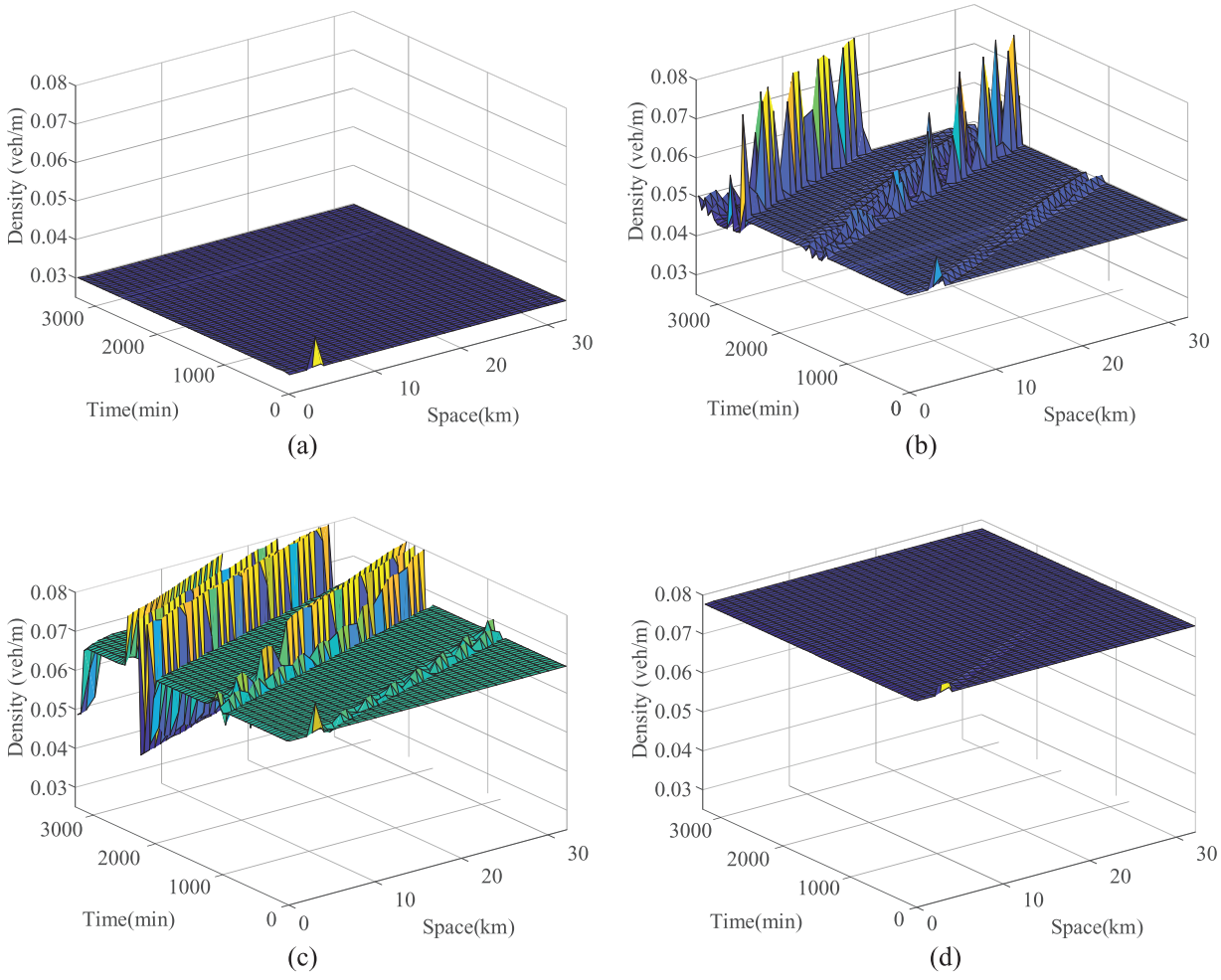

Fig. 3. The space–time evolution of small perturbation under different initial densities when $k_1 = 0.1$, $k_2 = 0.2$, $p = 0.2$, $\beta = 0.6$, $m = 1.5$, $b = 5$, (a) $\rho_0 = 0.03$; (b) $\rho_0 = 0.05$; (c) $\rho_0 = 0.067$; (d) $\rho_0 = 0.078$.

Solving the above equation, a feasible solution of above equation can be obtained

$$U = \frac{3\left(-mb_1\right)^2}{25\left(-m^2b_2\right)}\left[1 + 2\tanh\left(\pm\frac{-mb_1}{10m^2}\right) \times \left(X + \frac{6\left(-mb_1\right)^2}{25\left(-m^2b_2\right)}T + \zeta_0\right) + \tanh^2\left(\pm\frac{-mb_1}{10m^2}\right)\left(X + \frac{6\left(-mb_1\right)^2}{25\left(-m^2b_2\right)}T + \zeta_0\right)\right] \quad (36)$$

where ζ_0 represents an arbitrary constant.

5 Simulation example

In order to analyze the complex phenomenon of the new continuum model, the model (14) is first discretized based on the finite difference method, then the difference equation can be obtained:

$$\rho_i^{j+1} = \rho_i^j + \frac{\Delta t}{\Delta x}\rho_i^j\left(v_i^j - v_{i+1}^j\right) + \frac{\Delta t}{\Delta x}v_i^j\left(\rho_{i-1}^j - \rho_i^j\right) \quad (37)$$

– If the traffic is heavy, i.e. $v_i^j < c_i^j$

$$v_i^{j+1} = v_i^j - \frac{\Delta t}{\Delta x}\left(v_i^j - c_i^j\right)\left(v_{i+1}^j - v_i^j\right) + a\Delta t\left[V_e\left(\rho_i^j\right) - v_i^j\right] + \lambda_1 p\left(-v_i^j\right) + \Delta t\frac{k_2\left(1-p\right)m + b\beta}{2m\left(\Delta x\right)^2}\Delta^2\left(v_{i+1}^j - 2v_i^j + v_{i-1}^j\right) + \frac{\beta}{m\Delta x}\left[\left(v_{i+1}^{j+1} - v_{i+1}^j\right) - \left(v_i^{j+1} - v_i^j\right)\right]. \quad (38)$$

– If the traffic is light, i.e. $v_i^j \geq c_i^j$

$$v_i^{j+1} = v_i^j - \frac{\Delta t}{\Delta x}\left(v_i^j - c_i^j\right)\left(v_i^j - v_{i-1}^j\right) + a\Delta t\left[V_e\left(\rho_i^j\right) - v_i^j\right] + \lambda_1 p_n\left(-v_i^j\right) + \Delta t\frac{k_2\left(1-p\right)m + b\beta}{2m\left(\Delta x\right)^2}\Delta^2\left(v_{i+1}^j - 2v_i^j + v_{i-1}^j\right) + \frac{\beta}{m\Delta x}\left[\left(v_{i+1}^{j+1} - v_{i+1}^j\right) - \left(v_i^{j+1} - v_i^j\right)\right] \quad (39)$$

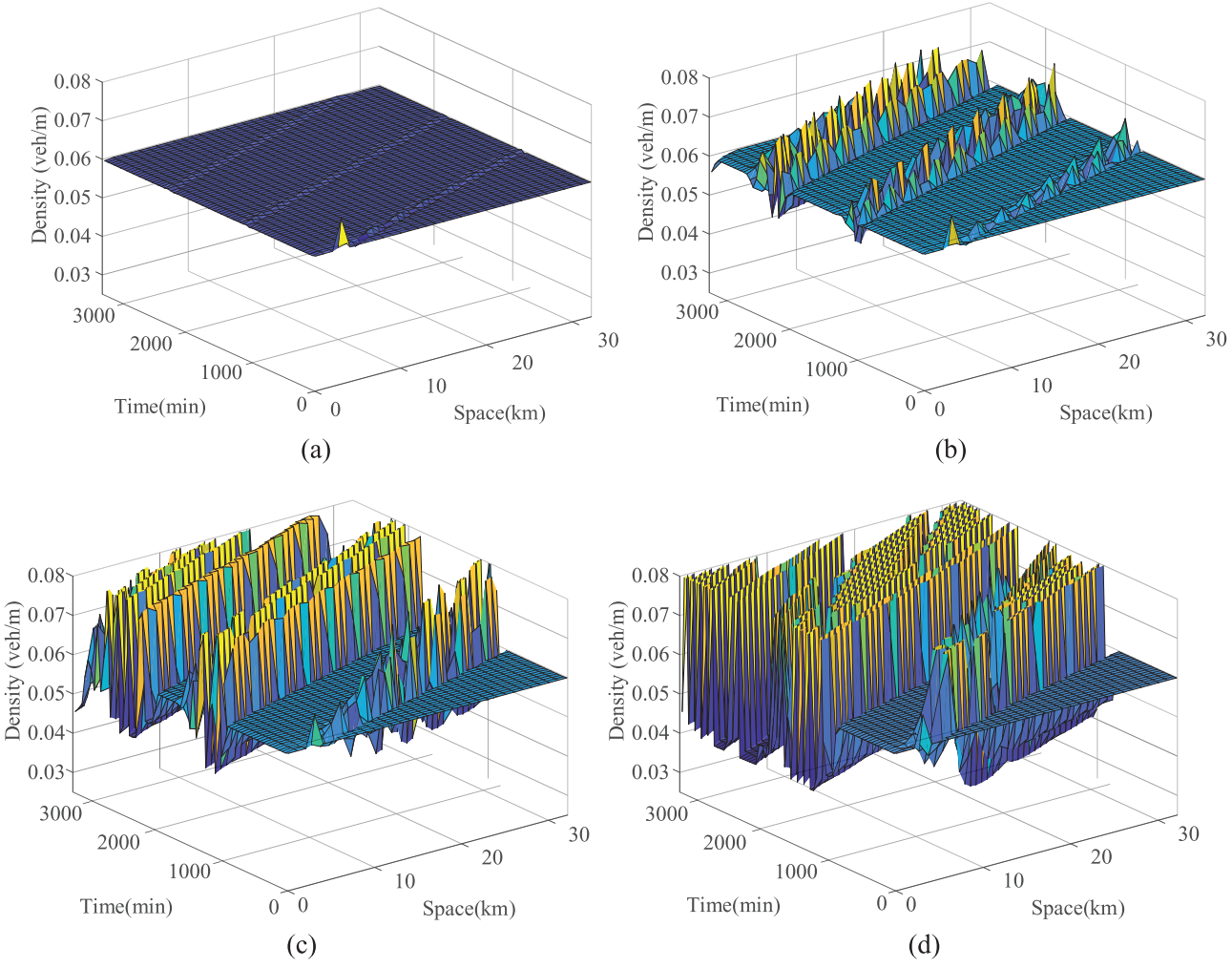

Fig. 4. The space–time evolution of small perturbation under different parameters p when $k_1 = 0.1$, $k_2 = 0.2$, $\rho_0 = 0.06$, $\beta = 0.6$, $m = 1.5$, $b = 5$ (a) $p = 0$; (b) $p = 0.3$; (c) $p = 0.5$; (d) $p = 0.7$.

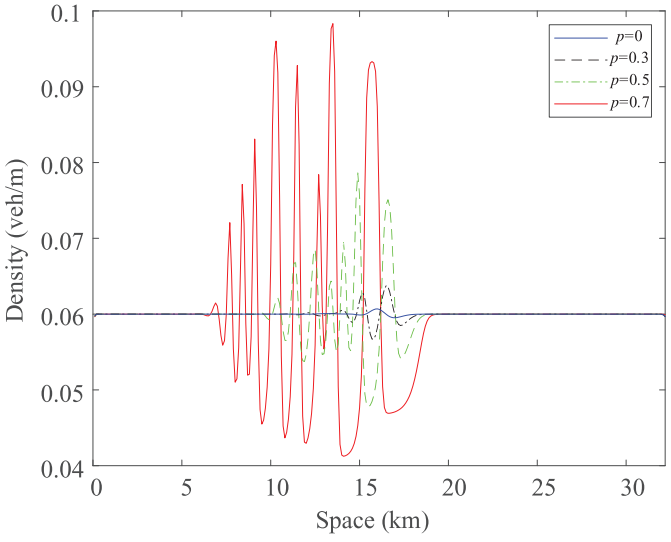

Fig. 5. Density profiles at $t = 800$ min corresponding to Figure 4.

where $c_i^j = \frac{k_2(1-p)m+b\beta}{m}\Delta + \frac{\beta}{m}\Delta\frac{v_{i+1}^j - v_i^j}{\Delta x}$; ρ_i^j, v_i^j represent the instantaneous density and instantaneous velocity of the vehicle on the road section i at time j respectively; Δx and Δt represent the spatial step and time step.

The average density ρ_0 given by Herrmann and Kerner in literature [63] is taken as the initial density of the sections on the road:

$$\rho(x,0) = \rho_0 + \Delta\rho_0 \left\{ \cos^{-2}\left[\frac{160}{L}\left(x - \frac{5L}{16}\right)\right] - \frac{1}{4}\cos^{-2}\left[\frac{40}{L}\left(x - \frac{11L}{32}\right)\right]\right\} \quad (40)$$

where the road length $L = 32.2$ km; $\Delta\rho_0$ is the density disturbance; the initial density of each section on the road is taken as the following period bounded condition.

$$\rho(L,t) = \rho(0,t), v(L,t) = v(0,t). \quad (41)$$

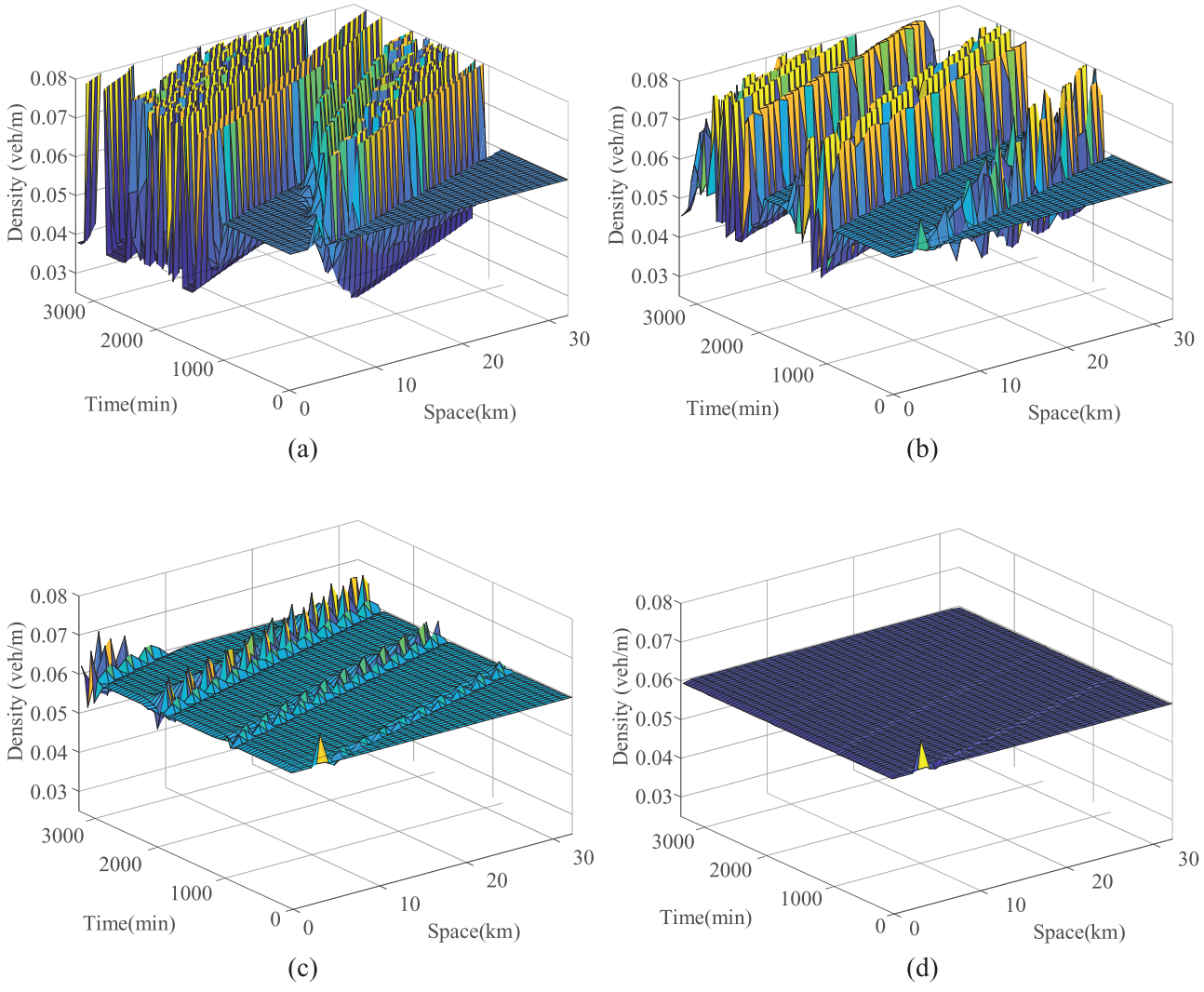

Fig. 6. The space–time evolution of small perturbation under different parameters β when $k_1 = 0.1, k_2 = 0.2$, $\rho_0 = 0.06$, $p = 0.3$, $m = 1.5, b = 5$, (a) $\beta = 0$; (b) $\beta = 0.6$; (c) $\beta = 0.9$; (d) $\beta = 1.2$.

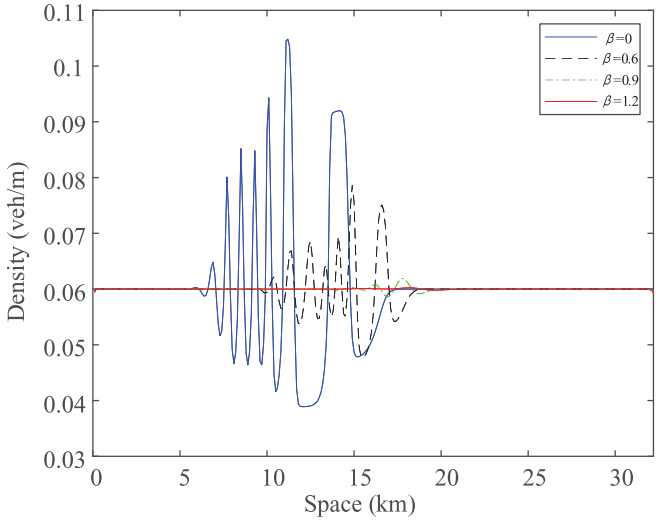

Fig. 7. Density profiles at $t = 800$ min corresponding to Figure 6.

We use the equilibrium velocity-density relationship proposed by Kerner and Konhauser [64].

$$v_e(\rho) = v_f \left[\left(1 + \exp \frac{\rho/\rho_m - 0.25}{0.06} \right)^{-1} - 3.72 \times 10^{-6} \right] \tag{42}$$

where v_f and ρ_m represent the free-flow velocity and the maximum density, respectively.

We assume that the initial flow on the road is in equilibrium, i.e. $u(x, 0) = V_e(\rho(x, 0))$. In order to facilitate subsequent analysis, we set the unit length is 100 meters, and the time cell is 1 seconds, the other related parameters of the model are set as follows:

$$\begin{aligned} &v_f = 30\,\text{m/s}, \rho_m = 0.2\,\text{veh/m}, \Delta x = 100\,\text{m}, \\ &T = 5\,\text{s}, a = 0.2, \Delta t = 1\,\text{s}, \Delta = 4. \end{aligned} \tag{43}$$

Figure 3 shows the spatiotemporal evolution of initial disturbance for different initial densities ρ_0. The other

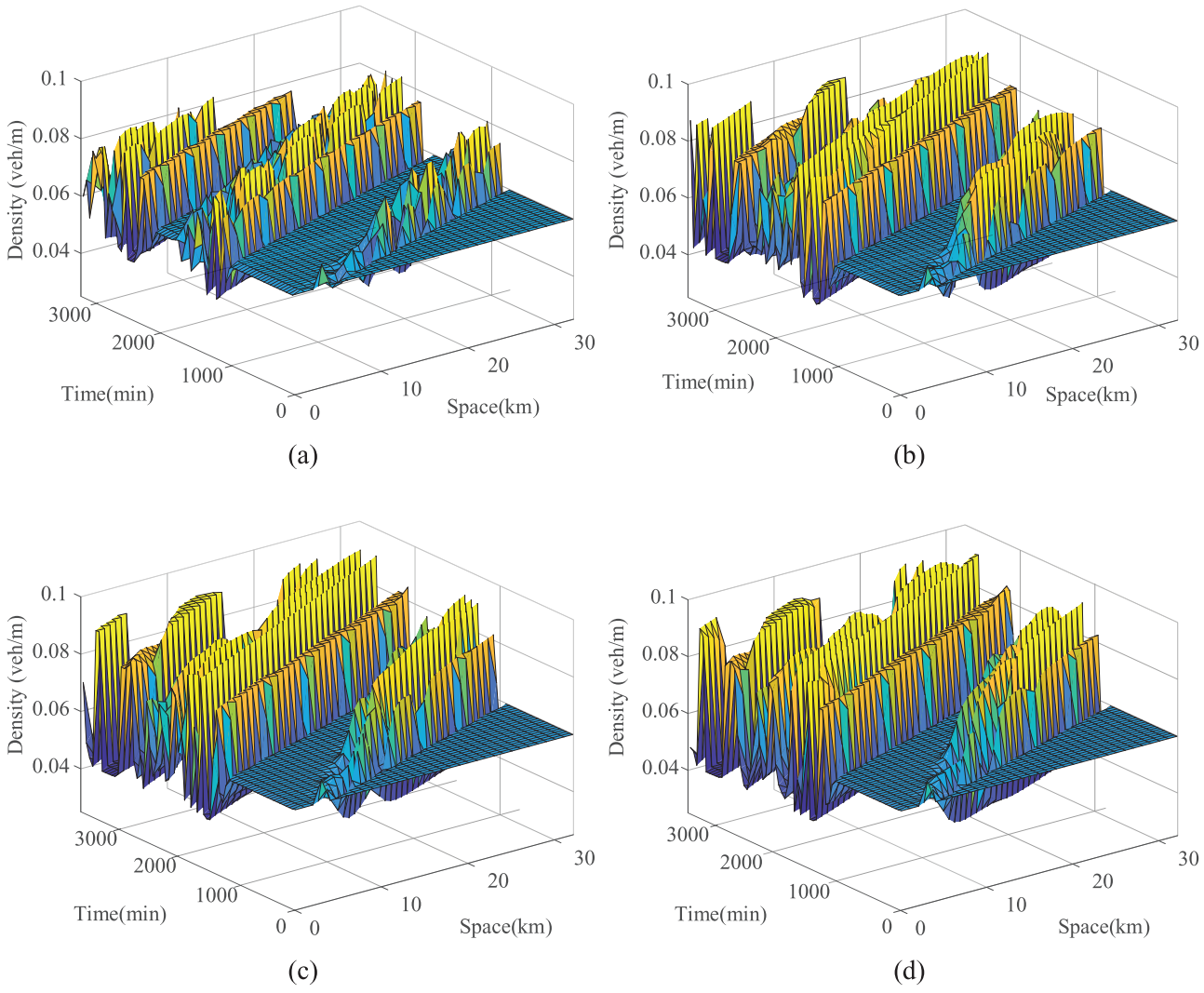

Fig. 8. The space–time evolution of small perturbation under different parameters m, (a) $m = 0.5$; (b) $m = 1$; (c) $m = 1.5$; (d) $m = 2$. ($k_1 = 0.1$, $k_2 = 0.2$, $b = 1$, $\beta = 0.6$, $\rho_0 = 0.06$, $p = 0.5$).

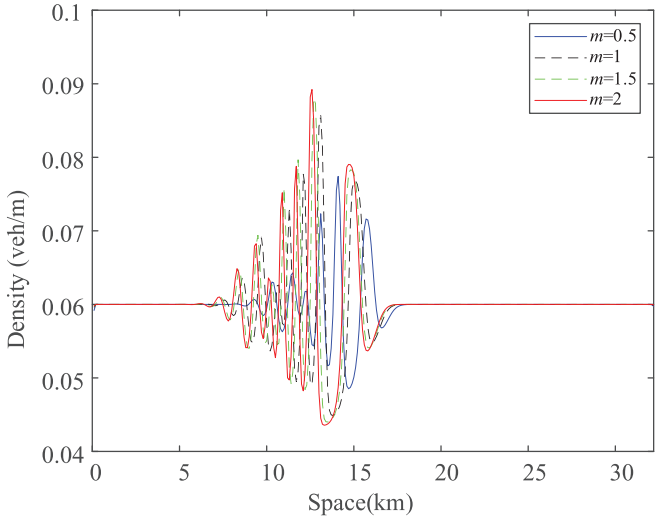

Fig. 9. Density profiles at $t = 800$ min corresponding to Figure 8.

parameters in our model are set as follows: $k_1 = 0.1$, $k_2 = 0.2$, $p = 0.2$, $\beta = 0.6$. From Figure 3a we found that the density fluctuation occurs when the initial density $\rho_0 = 0.03$. The stop-and-go wave occurs as the initial density ρ_0 increases. When the initial density increases to 0.05, the traffic flow evolves into multiple local clusters, which corresponding to stop-and-go traffic phenomenon. Finally, when the initial density exceeds 0.078, the density wave returns to the equilibrium state. Therefore, we conclude that: (1) initial density has a significant effect on the traffic flow stability; (2) 0.078 is an upper bound of the stable region; (3) when the initial density exceeds 0.078, the density wave remains stable; similarly, when the initial density is lower than 0.032, the density wave also keeps stable; (4) the unstable region of the initial density is 0.03 veh/m $< \rho_0 <$ 0.078 veh/m.

Figure 4 describes the evolution of initial disturbance under different parameter p, and the remaining parameters are taken as follows: $k_1 = 0.1$, $k_2 = 0.2$, $\rho_0 = 0.06$, $\beta = 0.6$, $m = 1.5, b = 5$. $p = 0$ indicates that no traffic

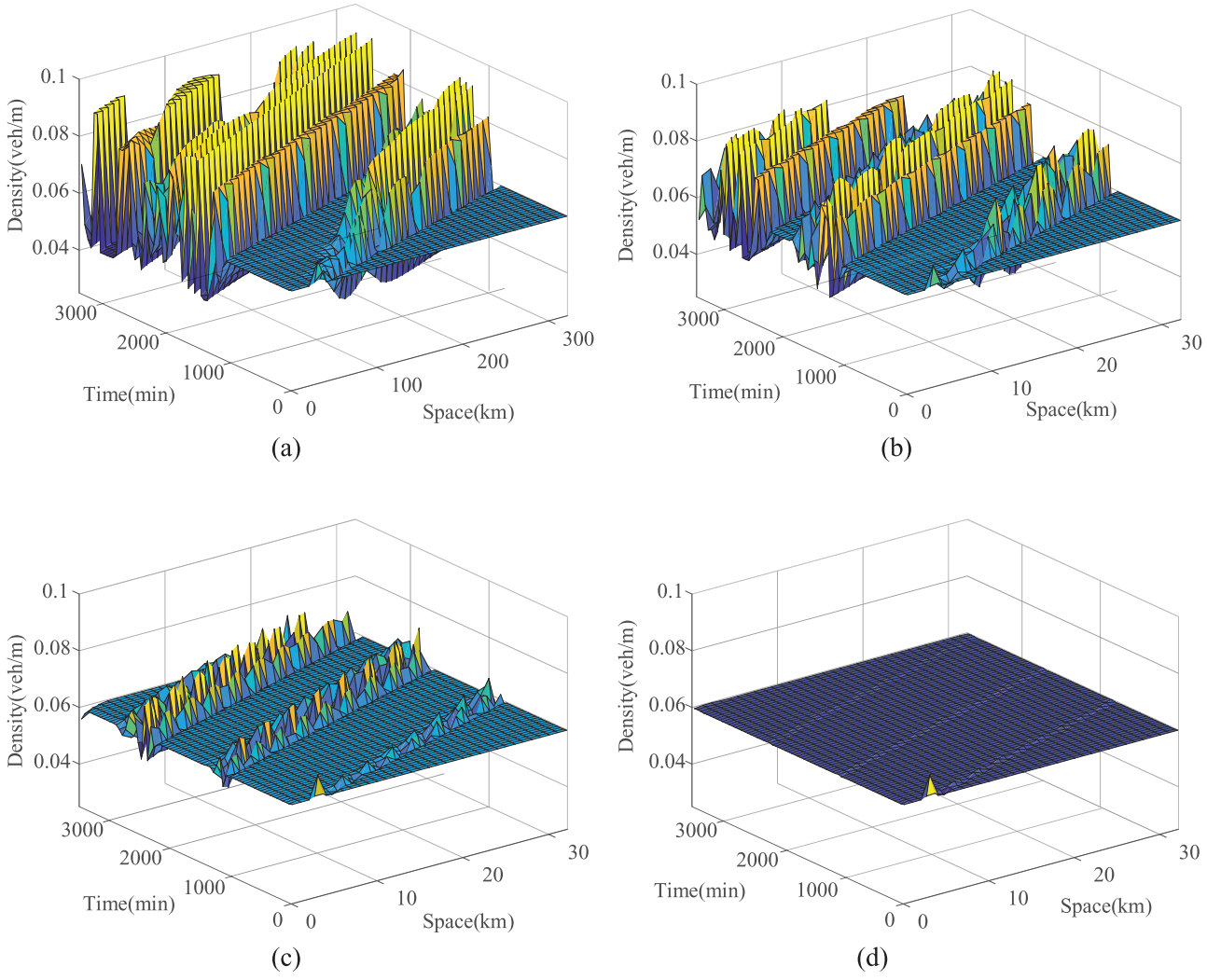

Fig. 10. The space–time evolution of small perturbation under different parameters b, (a) $m = 1.5$, $b = 1$; (b) $m = 1.5$, $b = 3$; (c) $m = 1.5$, $b = 5$; (d) $m = 1.5$, $b = 7$; ($k_1 = 0.1$, $k_2 = 0.2$, $\rho_0 = 0.06$, $p = 0.5$).

interruption exists in the continuum model. In this case, the current vehicle adjusts the velocity based on the velocity difference between the front vehicle and current vehicle, which collapses to Li's model [55]. As the parameter p increases, the traffic interruption probability is also higher. According to equation (5), at the interruption instance, the velocity information of the front vehicle cannot be obtained, such that the following vehicle is forced to stop to avoid rear collision. In this manner, the current vehicle adjusts its velocity using the inverse of current vehicle's speed as the control input, thereby exacerbating the speed difference between successive vehicles. As a result, the density fluctuating amplitude gradually increases with the increase of parameter p.

Figure 5 presents the instantaneous density distribution at time $t = 800$ min corresponding to Figure 3, from which we found that the fluctuation of traffic density is the lowest when $p = 0$, and the fluctuation of traffic density is the largest when $p = 0.7$. Combining Figures 4 and 5 we can conclude that the parameter p negatively correlates with the stability of traffic flow, which means that the traffic interruption will contribute inversely to the traffic flow stability.

Since β is the weight coefficient of the ET opening angle difference between consecutive vehicles, how this parameter affects the stability of traffic flow deserves some discussion. Figure 6 showcases the results. We found that when the weight coefficient β is higher, the likelihood of traffic flow oscillation is lower (and thus the traffic flow stability is stronger). This reinforces the message that taking into account the electronic throttle opening angle will enhance the stability of traffic flow. The explanation is as follows: during the driving process, the electronic throttle angle difference information will be converted into speed difference information and acceleration difference information based on equation (8). The information of speed and acceleration difference is then used for speed adjustment as the control input, which helps to stabilize the traffic flow.

Figure 7 shows the instantaneous density distribution at time $t = 1800$ min corresponding to Figure 6, which

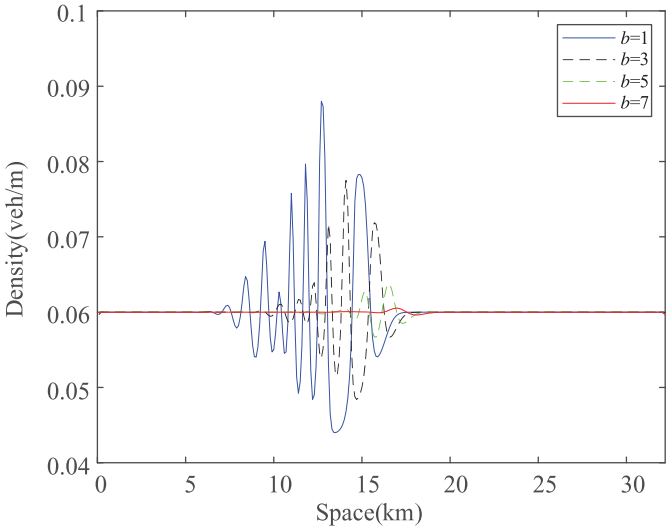

Fig. 11. Density profiles at $t = 800$ min corresponding to Figure 10.

indirectly verifies the conclusion from Figure 6. To sum up, the parameter β positively directly affect the stability of traffic flow.

Finally, we analyze the weight coefficient of velocity difference b and angle difference m on the performance of traffic flow. The results are shown in Figures 8–11. We observe that the parameter m and b present distinct effect on the stability of traffic flow. With the increase of parameter m, the amplitude of the oscillation caused by the initial disturbance is increased. This suggests that the parameter m contributes negatively to the stability of traffic flow. Adversely, the amplitude of density fluctuation decreases substantially with the increase of parameter b, and eventually disappeared when reaching a critical value as shown in Figure 10d. Therefore, the parameter b contributes to the stability of traffic flow.

6 Conclusion

With an expectation that CAVs are becoming commercially available in the future, there is imminent need to simulate the traffic flow and evaluate the impact of key components of control system that supports CAVs. In this paper, we proposed an extended continuum model considering the effect of traffic interruption probability and the electronic throttle opening angle in a connected vehicle environment. In linear and nonlinear analysis, the stability conditions and the KdV-Burgers equation of the new continuum model are obtained. In the simulation example, we found that the traffic interruption probability and the electronic throttle opening angle effect have a significant impact on the stability of traffic flow. Specifically, the electronic throttle angle difference information (parameter $\beta > 0$) contributes to the stability of traffic flow. The internal parameters m and b of electronic throttle contributes differently to the stability of traffic flow: the traffic flow is more stable with larger parameter m, whereas the traffic flow is less stable when the parameter b increases. The traffic interruption probability contributes negatively to the stability of traffic flow.

In the future, more realistic factors will be considered to improve the models, such as considering drivers' characteristics and lane-changing behaviour. In addition, data acquisition and model validation is an interesting work.

This work is partly supported by the Youth Innovation Talents Funds of Colleges and Universities in Guangdong Province (Project No. 2018KQNCX287), the Foshan Self-funded Technology Project (No. 2018AB003651), the National Science Foundation of China (Project No. 61703165), and Science and Technology Program of Guangzhou, China (Project No. 201904010202).

Author contribution statement

Cong Zhai: conceptualization, methodology, writing – original draft. Weitiao Wu: conceptualization, methodology, writing – review & editing, supervision.

References

1. W. Wu, R. Liu, W. Jin, Transp. Res. B **93**, 95 (2016)
2. W. Wu, R. Liu, W. Jin, Trans. Res. B **104**, 175 (2017)
3. W. Wu, R. Liu, W. Jin, C. Ma, Tran. Res. B **121**, 275 (2019)
4. W. Wu, R. Liu, W. Jin, C. Ma, Tran. Res. E **130**, 61 (2019)
5. A. Gupta, V. Katiyar, Transportmetrica **3**, 73 (2007)
6. A. Gupta, V. Katiyar, J. Phys. A **38**, 4069 (2005)
7. A. Gupta, S. Sharma, Chin. Phys. B **1**, 299 (2012)
8. A. Gupta, S. Sharma, Chin. Phys. B **11**, 156 (2010)
9. A. Gupta, Int. J. Mod. Phys. C **24**, 50018 (2013)
10. A. Gupta, I. Dhiman, Nonlinear Dyn. **79**, 663 (2015)
11. A.K. Gupta, S. Sharma, P. Redhu, Commun. Theor. Phys. **62**, 393 (2014)
12. P. Redhu, A.K. Gupta, Physica A **421**, 249 (2015)
13. C. Zhai, W. Wu, Mod. Phys. Lett. B **32**, 1 (2018)
14. C. Zhai, W. Wu, Clust. Comput. **22**, 7447 (2019)
15. C. Zhai, W. Wu, Int. J. Mod. Phys. C **2020**, 2050031 (2020)
16. C. Zhai, W. Wu, Mod. Phys. Lett. B **33**, 2050071 (2020)
17. S. Sharma, Physica A **421**, 401 (2015)
18. S. Sharma, Nonlinear Dyn. **81**, 991 (2015)
19. A.K. Gupta, P. Redhu, Physica A **392**, 5622 (2013)
20. L. Zheng, S. Ma, S. Zhong, Physica A **390**, 1072 (2011)
21. J.P. Meng, S.Q. Dai, L.Y. Dong et al., Physica A **380**, 470 (2007)
22. H.X. Ge, X.P. Meng, H.B. Zhu et al., Physica A **408**, 28 (2014)
23. D. Yang, P. Jin, Y. Pu et al., Physica A **395**, 371 (2014)
24. L. Zheng, S. Zhong, P.J. Jin et al., Physica A **391**, 5948 (2012)
25. M. Bando, K. Hasebe, A. Nakayama et al., Phys. Rev. E **51**, 1035 (1995)
26. B.G. Cao, Physica A **427**, 218 (2015)
27. D.W. Liu, Z.K. Shi, W.H. Ai, Commun. Nonlinear Sci. Numer. Simul. **47**, 139 (2017)
28. S. Yu, Z. Shi, Physica A **428**, 206 (2015)
29. F. Lv, H.B. Zhu, H.X. Ge, Nonlinear Dyn. **77**, 1245 (2014)
30. C. Zhai, W. Wu, Mod. Phys. Lett. B **32**, 1850382 (2018)

31. L.J. Zheng, C. Tian, D.H. Sun et al., Nonlinear Dyn. **70**, 1205 (2012)
32. H.X. Ge, F. Lv, P.J. Zheng et al., Nonlinear Dyn. **76**, 1497 (2014)
33. C. Zhai, W. Wu, Int. J. Mod. Phys. C **30**, 1959973 (2019)
34. Y. Jin, M. Xu, Physica A **459**, 107 (2016)
35. S. Li, L. Yang, Z. Gao et al., Isa Trans. **53**, 1739 (2014)
36. G. Peng, Q. Li, Mod. Phys. Lett. B **30**, 1650243 (2016)
37. Y. Zhang, P. Ni, M. Li et al., J. Adv. Trans. **2017**, 1 (2017)
38. C. Zhai, W. Wu, Nonlinear Dyn. **2018**, 1 (2018)
39. D.H. Sun, X.Y. Liao, G.H. Peng, Physica A **390**, 631 (2011)
40. G.H. Peng, Chin. Phys. B **19**, 434 (2010)
41. D.H. Sun, X.Y. Liao, G.H. Peng, Physica A **390**, 631 (2011)
42. G.H. Peng, D.H. Sun, Phys. Lett. A **374**, 1694 (2010)
43. G.H. Peng, X.H. Cai, C.Q. Liu et al., Phys. Lett. A **375**, 3973 (2011)
44. G.H. Peng, R.J. Cheng, Physica A **392**, 3563 (2013)
45. F. Liu, R. Cheng, H. Ge et al., Nonlinear Dyn. **85**, 1469 (2016)
46. F. Liu, R. Cheng, P. Zheng et al., Nonlinear Dyn. **83**, 1 (2016)
47. C. Zhai, W. Wu, Phys. Lett. A **382**, 3381 (2018)
48. L. Yi, R.J. Cheng, L. Li et al., Physica A **463**, 376 (2016)
49. T. Tang, W. Shi, H. Shang et al., Nonlinear Dyn. **76**, 2017 (2014)
50. S. Yu, Q. Liu, X. Li, Commun. Nonlinear Sci. Numer. Simul. **18**, 1229 (2013)
51. J. Zhao, P. Li, Physica A **473**, 178 (2017)
52. Y.J. Liu, H.L. Zhang, L. He, Chin. Phys. Lett. **29**, 104502 (2012)
53. J. Monteil, R. Billot, J. Sau et al., IEEE Trans. Intell. Trans. Syst. **15**, 2001 (2014)
54. H. Liu, D. Sun, M. Zhao, Nonlinear Dyn. **84**, 881 (2016)
55. Y.L. Jiao, H.X. Ge, R.J. Chen, Physica A **535**, 122362 (2019)
56. Y. Li, H. Yang, B. Yang et al., Nonlinear Dyn. **93**, 1923 (2018)
57. D. Helbing, B. Tilch, Phys. Rev. E **58**, 133 (1998)
58. R. Jiang, Q. Wu, Z. Zhu, Phys. Rev. E **64**, 017101 (2001)
59. T.Q. Tang, H.J. Huang, S.J. Huang et al., Chin. Phys. B **387**, 975 (2009)
60. R. Cheng, H. Ge, J. Wang, Phys. Lett. A **381**, 2792 (2017)
61. R. Cheng, J. Wang, H. Ge et al., Mod. Phys. B **32**, 1850037 (2018)
62. N. Davoodi, A.R. Soheili, S.M. Hashemi, Nonlinear Dyn. **83**, 1621 (2016)
63. H. Liu, P. Zheng, K. Zhu et al., Physica A **438**, 26 (2015)
64. R. Jiang, Q.S. Wu, Z.J. Zhu, Trans. Res. B **36**, 405 (2002)